# Structural Investigations of Oriented Membrane Assemblies by FTIR-ATR Spectroscopy*

Urs Peter Fringeli[1], Jeannette Goette[2], Gerald Reiter[1], Monira Siam[1], and Dieter Baurecht[1]

[1] *Institute of Physical Chemistry, University of Vienna, Althanstrasse 14, A-1090 Vienna, Austria.*
[2] *Medinova AG, Eggbühlstrasse 14, CH-8050 Zurich, Switzerland.*

*In situ* attenuated total reflection (ATR) Fourier transform (FT) spectroscopy is presented as an adequate tool for studying molecular structure and function of biomembranes. In this article emphasis was directed to the production of suitable model bilayer membranes for optimum mimicking of natural biomembranes, and to special FTIR ATR techniques to achieve enhanced selectivity as well as time resolved information on complex membrane assemblies. In this context, the preparation of supported bilayers according to the LB/vesicle method is presented and the use of such model membranes to build more complex assemblies, e.g. with creatine kinase, a surface bound enzyme, and alkaline phosphatase, a membrane anchored enzyme. A comprehensive summary of equations used for quantitative ATR spectroscopy is given and applied to determine the surface concentration and orientation of membrane bound molecules. The use of supported bilayers for drug membrane interaction studies is demonstrated by the local anesthetic dibucaine. Besides of structural information's, such studies result also thermodynamic date, such as adsorption isotherm and partition coefficient. A special ATR set-up for more precise background compensation is presented enabling the conversion of a single beam spectrometer into a pseudo double beam spectrometer. This optical component may be placed in the sample compartment of the spectrometer, and is referred to as single-beam-sample-reference (SBSR) attachment. Finally, a short theoretical introduction into time resolved modulation spectroscopy is given. Temperature modulated excitation of reversible conformational changes in the polypeptide poly-L-lysine and the enzyme RNase are shown as examples.

## INTRODUCTION

Biological model membranes in the form of planar supported bilayer assemblies are of special interest for attenuated total reflection spectroscopy (ATR), since the internal reflection element (IRE) may act as both, the solid support and the wave guide. This set up enables membrane spectroscopy from the part of the solid support, and simultaneous control of the membrane environment from the opposite part. Moreover, the supported membrane is located in the most intense region of the electric field of the evanescent wave which favors the fraction of light absorbed by the membrane with respect to unwanted absorption's of the background (e.g. buffer solution). Oriented regions of the assembly, which should be expected because of intrinsic ordering of lipid bilayers, may be detected and analyzed in a straightforward way by the use of polarized incident light.

Several methods have been described in the literature to prepare symmetric or asymmetric lipid bilayers. Among them the three most important one should be noted: (i) The Langmuir-Schaefer method, adapted for model membrane studies by Tamm and McConnell (1). A hydrophilic plate was coated by a Langmuir-Blodgett (LB) monolayer of a phospholipid. The hydrophobic surface of the supported monolayer was then contacted with the corresponding hydrophobic surface of a compressed monolayer at the air water interface of a film balance. Immersing this plate in vertical direction into the subphase results in the supported bilayer in the aqueous environment of the subphase. (ii) A different way to get supported bilayers was described by Brian and McConnell (2). A dispersion of small unilamellar lipid vesicles is brought into contact with the hydrophobic surface of a solid support, leading to a spontaneous spreading of the vesicles on the solid. (iii) The best characterized procedure leading to supported bilayers is the so called LB/vesicle method (3), (4), (5), (6). As in the first case, the ATR plate (IRE) is coated by a LB lipid monolayer pointing with the hydrocarbon chains towards the air. This plate is now mounted in an ATR flow-through cell where it is contacted by an aqueous solution of lipid vesicles. Since a hydrophobic surface exhibits a large surface energy when in contact with liquid water, a spontaneous oriented adsorption of lipid molecules from the vesicles to the LB monolayer takes place leading to a stable bilayer membrane. Adsorption may be monitored *in situ* by IR ATR spectroscopy.

So far a variety of experiments with different types of supported lipid membranes have been reported for the interaction with proteins, peptides and drugs. First use was made by studying the interaction of local anesthetics (LA) of the tertiary amine type with a dipalmitoylphosphatidic acid (DPPA)/palmitoyl-oleoyl-phosphatidylcholine (POPC) lipid bilayer where POPC was facing the liquid environment (7).

*) In memorial of Robert Kellner

In order to probe the degree of penetration of the LA dibucaine (DIBU) into the lipid bilayer, as well as the influence on hydrocarbon chain ordering in the membrane, a supported bilayer was used, consisting of DPPA as inner monolayer and dimyristoyl-phosphatidylcholine with deuterated hydrocarbon chains (DMPC-$d_{54}$) as outer layer facing the aqueous environment (8), (9). In another application, a supported DPPA/POPC bilayer served by itself as a support for natural membrane fragments enriched with the $Na^+/K^+$-ATPase (sodium-potassium pump) (10). The orientation of the peptide melittin in a POPC/POPG (POPG: Palmitoyl-oleoyl-phosphatidylglycerol) was studied by means of FTIR ATR spectroscopy using polarized incident light (11). This study revealed that the structure of melittin as well as its orientation with respect to the membrane critically depends on the degree of hydration. A similar behavior was observed with the antibiotic alamethicin which was incorporated into dipalmitoyl-phosphatidylcholine (DPPC) mulibilayers (12). Obviously, the structures of oligopeptides are very sensitive to the environment. As a consequence, fully hydrated membrane assemblies must be considered as the most adequate models for ATR spectroscopy. In this respect, it is of great importance to have a good characterization of the supported bilayer from different points of view. In addition to FTIR studies (refs. 3 - 6) valuable information on the nano-structure was obtained by combined application of FTIR and atomic force microscopy (AFM) (13) since nano- and ultra-structure of a sample are of utmost importance for a reliable interpretation of polarized spectra. A further critical point when working with supported bilayers is the lateral mobility of lipid molecules in the inner (LB) monolayer. Fluorescence recovery after photo bleaching (FRAP) has revealed that the lateral mobility of natural phospholipids is preserved (5) giving good evidence for a significant water layer between the solid support (IRE) and the immobilized membrane.

In this presentation we discuss the preparation and characterization of three membrane systems. Two enzyme-membrane assemblies, the mitochondrial creatine kinase (CK) interacting with cardiolipin (CL), and the alkaline phosphatase (AP) interacting with POPC, as well as dibucaine (DIBU), a local anesthetic interacting with a DPPA/POPC bilayer.

Physiologically, the mitochondrial CK is important for the energy metabolism in cells of high and fluctuating energy requirements. The native form of the enzyme is octameric and highly ordered as revealed by x-ray diffraction (14). Typical features are a large channel, connecting the top to the bottom face of the nearly cubic shaped octamer and the accumulation of positively charged residues at these opposite faces. CK was found to adsorb spontaneously to negatively charged phospholipid membranes most probably by one of the positively charged surfaces. First kinetic results have been obtained by plasmon resonance and light scattering experiments (15). *In situ* FTIR ATR spectroscopy with polarized light was used to monitor the formation of a membrane assembly consisting of a DPPA/CL bilayer membrane and the binding of CK to this membrane. Quantitative analysis resulted in a surface coverage of about 60% by CK (16). Furthermore, a flow-through system enabled the measurement of enzyme activity simultaneously with spectroscopic data acquisition. Structural changes in the lipid bilayer revealed a predominant electrostatic interaction at the membrane surface (17).

In contrast, the alkaline phosphatase (AP) is a dimeric enzyme with one glycosyl-phosphatidylinositol (GPI) molecule covalently bound to each subunit. The hydrophobic hydrocarbon chains of the phospholipid are responsible for anchoring the enzyme in the lipid bilayer. AP is insoluble in aqueous buffer solution and needs addition of a detergent for solubilization. On the other hand structure and stability of the supported lipid bilayer are influenced, too. Detachment from the IRE was observed as soon as the detergent concentration was equal or higher than the critical micelle concentration (cmc). Obviously, the transfer of AP from solution to the lipid bilayer is much more critical than that of CK. *In situ* measurements of the formation and characterization of the membrane assembly consisting of an inner DPPA LB-layer with an adsorbed POPC layer and bound AP have been performed. A considerable amount POPC molecules from the outer leaflet of the bilayer were found to be replaced by detergent molecules (β-octylglucoside, β-OG) during AP attachment to the bilayer membrane. Moreover, the hydrocarbon chain ordering of the inner membrane leaflet (DPPA) was decreased upon AP binding giving evidence for a hydrophobic interaction, possibly with the GPI anchor (18).

The interaction of DIBU, a tertiary amine local anesthetic (LA) with a supported bilayer membrane consisting of a DPPA inner leaflet and a POPC outer leaflet was studied *in situ* at different DIBU concentrations. Even at bulk pH 5.5 where the amino group of dissolved DIBU, which has a pK value of 8.9, is nearly completely protonated, quantitative FTIR ATR measurements revealed that about 50% of the membrane bound DIBU was in the deprotonated, i.e. in a hydrophobic, water insoluble state. This approximately 1:1 mixture of charged and uncharged DIBU is assumed to be characteristic of aggregated DIBU. A small fraction of the total amount of detected uncharged DIBU is expected to be in the interior of the lipid bilayer. This finding is supported by the observation that the hydrocarbon chain ordering of both, the outer (POPC or DMPC-$d_{54}$), and the inner (DPPA) m were significantly reduced compared to the ordering in an unperturbed supported bilayer. The majority of uncharged DIBU, however, is expected to be aggregated with the protonated (charged) form, even without influence of the membrane.

A new ATR attachment will be presented, too. It enables the conversion of a single beam (SB) spectrometer into a pseudo double beam instrument in order to achieve more stable background compensation than with the conventional SB technique. This attachment converts convergent light

entering the sample compartment into a parallel beam. The latter is focused to the entrance of a multiple internal reflection element (MIRE) by means of a cylindrical mirror thus producing a parallel ray propagation within the MIRE (wave guide). Placing now the sample at the lower half of the plate and the reference at the upper half and switching the beam by a chopper alternatively up and down leads to the so-called single beam sample reference (SBSR) technique (3), featuring two advantages over conventional SB technique: (i) elimination of water vapor incompensation, and (ii) compensation of drifts resulting from the instrument or the sample/reference, respectively. In this article we present a SBSR ATR attachment which makes use of a computer controlled lift in order to move the upper or lower half of the MIRE into the parallel beam. This set up leads to a better base line than the chopper version used earlier (3,4) since the FTIR spectrometer turned out to have inhomogeneous intensity within the cross-section of the IR beam. Subdividing this beam into an upper and lower half and calculating the ratio of the corresponding single channel spectra will therefore not result in a flat 100% line as should be expected for an ideal spectrometer.

Finally, an outlook to the application of more sophisticated dynamic techniques such as modulated excitation (ME) FTIR spectroscopy is given. External periodic stimulation of the membrane assembly may be accomplished via thermodynamic parameters such as temperature (T), concentration (c), electric field (E), light flux ($\Phi$) etc. The power of ME-FTIR spectroscopy is based on the one hand on a significant enhancement of the selectivity of the measurement which is of great importance in the case of macromolecule spectroscopy featuring heavily overlapped absorption bands. Selectivity is achieved by the fact that only molecules or molecular parts (e.g. functional groups) affected by the periodic external perturbation will result in a corresponding modulated absorbance spectrum. Phase sensitive detection (PSD) enables now a separation of modulated and non-modulated parts of the FTIR spectrum with a higher accuracy than achieved by conventional difference spectroscopy.

Moreover, if the system response to a sinusoidal excitation with frequency $\omega$ contains not only the fundamental $\omega$, but also the first harmonic ($2\omega$) or even higher harmonics, one has unambiguous evidence for a nonlinear chemical system,which may originate in chemical reactions different from first order and/or cooperative phenomena. The latter are of special interest in processes where conformational changes of biological macromolecules are involved. If a time resolved data acquisition of the system response is possible, a kinetic analysis of the process may be performed on the basis of the frequency dependence of both, amplitudes and phases of modulated absorbances of the system response. This information is accessible by phase sensitive detection (PSD) of time resolved FTIR absorbance spectra via analog or digital procedures (19). Variation of the modulation frequency $\omega$ results in independent data sets which facilitate the reconstruction of the reaction scheme. This is the main advantage of ME spectroscopy on relaxation (REL) spectroscopy. Although both, ME and REL techniques have the same physico-chemical information content, the read out of this information, however, is facilitated by ME, because more independent experimental data is available due to the additional degree of freedom given by the parameter 'modulation frequency' $\omega$, while the number of unknown kinetic parameters included the reaction scheme are the same for ME and REL. After a theoretical introduction to ME spectroscopy, T-ME spectra of poly-L-lysine (PLL) will be shown. PLL may be converted reversibly from the $\alpha$-helical to the antiparallel $\beta$-pleated sheet structure by T-modulation under adequate conditions. At least three so far unknown transient species have been detected and sequentially assigned based on their phase shift with respect to the T-stimulation (20). Finally, preliminary results from a T-modulation experiment performed with RNase A is shown. This enzyme undergoes a reversible unfolding/refolding process with a distinct transition temperature at T=64°. Time resolved temperature jump (T-jump) measurements revealed relaxation times in the range of $\tau_i$ = 5-10 s (21). A corresponding T-ME experiment has been performed by switching the temperature between 59°C and 69°C with a period $\tau_{mod}$ = 25 s.

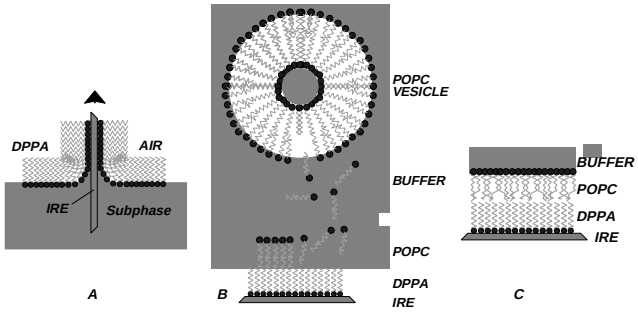


**FIGURE 1 .** Supported lipid membrane prepared by the LB/vesicle technique. **A**: The solid support (IRE) is coated by a lipid monolayer (e.g. DPPA) transferred in the compressed state from the air-water interface of a film balance by means of the Langmuir-Blodgett technique. **B**: Spontaneous lipid transfer from vesicles (e.g. POPC) to the hydrophobic surface of the LB monolayer occurs by forming a supported bilayer. **C**: Completed asymmetric bilayer ( e.g. DPPA/POPC) in contact with buffer solution.

## PREPARATION OF SUPPORTED MODEL MEMBRANE ASSEMBLIES

### Supported Bilayers

Model bilayers for *in situ* ATR studies have been prepared according to the LB/vesicle method. The principle steps of this procedure are depicted in Fig. 1.

In practice, after LB-layer transfer, see Fig. 1A, the monolayer coated IRE is mounted in an ATR flow through cuvette as depicted by Fig. 2. After spectroscopic examination of quantity and quality (ordering) of the LB monolayer a vesicle solution of any phospholipid is circulated through the cuvette. This set up enables direct monitoring of the state of lipid adsorption shown by Fig. 1B.

After about 30 min the state of Fig. 1C is reached. A special washing procedure turned out to be necessary in order to detach loosely bound vesicle fragments. For details, the reader is referred to refs. (4), (6) and (16).

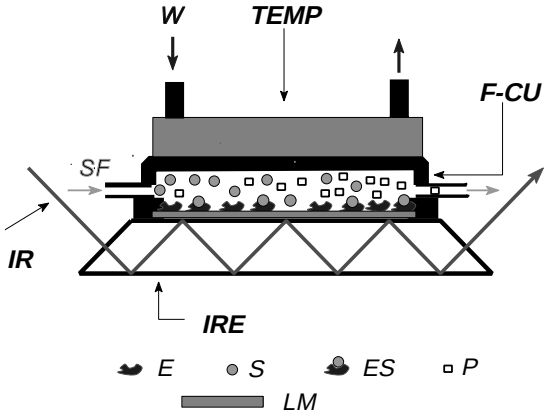


**FIGURE 2.** Flow-through cuvette (F-CU) for *in situ* FTIR ATR spectroscopy. The IRE is coated by a supported bilayer (LM) to whom the enzyme (E) is immobilized. The substrate (S) flowing through the cuvette (SF) is enzymatically converted into the product (P).

### Membrane Bound Creatine Kinase

Mitochondrial creatine kinase (CK) is a highly ordered octamer. It has nearly cubic shape with an edge of 93 Å (14) and features an accumulation of positive charges at two opposite sides of the cube. Probably one of these sides binds to the membrane surface, predominantly by electrostatic interaction. Therefore, a DPPA/CL membrane (CL: cardiolipin) was used where CL formed the outer negatively charged layer of the supported bilayer. Pumping CK through the ATR flow-through cuvette (Fig. 2) lead to a spontaneous adsorption of CK. The observed surface coverage of 60 % and the kinetics of CK adsorption were in accordance with results obtained by a plasmon resonance study (15). For details the reader is referred to ref. (16).

### Membrane Anchored Alkaline Phosphatase

Alkaline phosphatase (AP) is also a membrane bound enzyme. The binding mechanism of AP, however, is quite different from that of CK. Native AP forms a water insoluble dimer where each monomer has one covalently bound glycosyl phosphatidylinositol (GPI) phospholipid molecule. It is assumed that AP is anchored to a bilayer predominantly via the hydrocarbon chains of GPI, penetrating into the hydrophobic region of the bilayer. Consequently, the reconstitution of a membrane assembly with bound AP must be expected to be more delicate than with CK. Indeed, the detergent β-octylglucoside (β-OG) which was added in order to solubilize AP has lead to the fist problem, because it destroyed the POPC layer of a DPPA/POPC bilayer nearly completely. FTIR spectra revealed, however, that the spectra of AP and β-OG appeared at the place of POPC. In a second step it was possible to exchange β-OG by POPC using an aqueous buffer solution with POPC vesicles circulating through the ATR cuvette. For a more detailed discussion, the reader is referred to ref. (16).

## QUANTITATIVE ATR SPECTROSCOPY

### Evanescent Wave and Penetration Depth

The relevant optical parameters are depicted by Fig. 3, which shows schematically the trace of a ray upon internal reflection at the membrane IRE interface. The goal of this analysis of FTIR ATR spectra is the calculation of the surface concentration and orientation of molecules in an

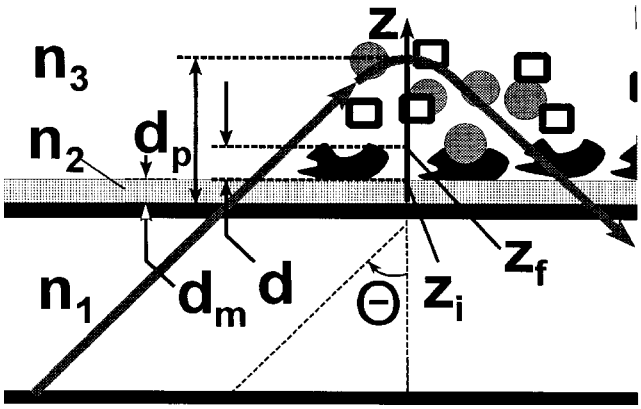


**FIGURE 3.** Penetration depth $d_p$ of the evanescent wave**.** The internally reflected light propagates within the IRE (index 1) with an angle of incidence θ. It penetrates the membrane (index 2) of thickness $d_m \approx 50$ Å and the adsorbed enzyme (adlayer of thickness d, ranging from $z = z_i$ to $z = z_f$) and enters the aqueous environment (index 3). The strength of the electric field decreases exponentially with distance z from the 1-2 interface, see eqn. 1. The refractive indices of the media are denoted by $n_1$, $n_2$, and $n_3$.

adsorbed layer as well as the bulk concentration of dissolved substances in the aqueous environment. For that purpose some characteristic properties of internal reflection spectroscopy must be explained. Fig. 4 shows the IRE fixed coordinate system which is relevant for the description of optical and structural features of the system. Straightforward calculation of the propagation of a plane wave from medium 1 (IRE) into a nonabsorbing medium 2 under the conditions of total reflection (22) yields eqn. (1)

$$E_{x,y,z,2}(z) = E_{x,y,z,2}(0)\exp(-z/d_p) \qquad (1)$$

It follows that all electric field components of the so-called evanescent wave decrease exponentially with distance z from the interface. $d_p$ denotes the penetration depth, which according to eqn. (2) is in the order of the wavelength of the light in the medium 1. The relative field components at the interface 1-2, $E^r_{x,y,z,2}(0) = E^r_{0x,0y,0z,2}$ may be calculated by Fresnel's equations (refs. (4),(22),(23), eqn. (7)).

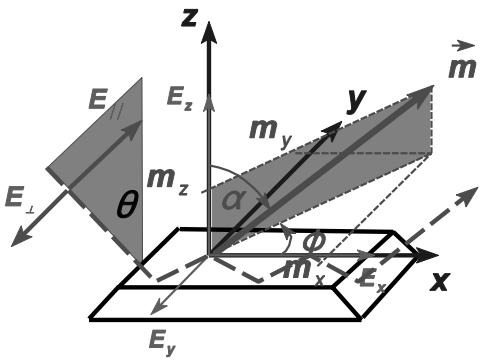


**FIGURE 4.** ATR set up. Optical and structural features are related to the IRE fixed coordinate system x,y,z. $E_{||}$ and $E_{\perp}$ denote the parallel and perpendicular polarized components of the light incident to the IRE under the angle θ. $E_{||}$ results in the $E_x$, and $E_z$ components of the evanescent field, while $E_{\perp}$ results in the $E_y$ component. $\vec{m}$ denotes the unit vector in direction of the transition dipole moment vector of a given vibrational mode, and $m_x$, $m_y$, $m_z$ are the corresponding components in the IRE coordinate system. $\vec{m}$ goes off at an angle α with respect to the z-axis and the projection of $\vec{m}$ to the xy-plane goes off at an angle ϕ with respect to the x-axis.

$$d_p = \frac{\lambda/n_1}{2\pi(\sin^2\theta - (\frac{n_3}{n_1})^2)^{\frac{1}{2}}} \qquad (2)$$

$\lambda_1 = \lambda/n_1$ denotes the wavelength in medium 1, and λ is the vacuum wavelength. θ is the angle of incidence. Since the thickness of the membrane assembly is in the range of 50 Å to 150 Å, i.e. only about 1 % of the penetration depth, the electric field in the rarer medium is predominantly determined by the bulk medium 3. Therefore, the refractive index $n_3$, is used instead of $n_2$, see Fig. 3. This is the basic assumption for the thin layer approximation introduced by Harrick (23). As a consequence the electric field in the membrane (thin medium 2) is then assumed to be determined by the boundary conditions valid for a thin dielectric film in the electric field of the evanescent wave generated by the bulk media 1 and 3, see refs. (4) and (23).

## Effective thickness $d_e$

The concept of effective thickness has been introduced by Harrick, ref. (23). The quantity $d_e$ indicates the thickness of a sample that would result in the same absorbance in a hypothetical transmission experiment, as obtained with the genuine ATR experiment. This concept enables application of Lambert-Beer's law on ATR spectra according to eqn. (3).

$$T = 10^{-\varepsilon c d_e} = 10^{-A} \qquad (3)$$

where $A = \varepsilon c d_e$ denotes the absorbance per internal reflection. For an isotropic layer extended from $z = z_i$ to $z = z_f$ one obtains (ref. (4)).

$$d_e^{iso} = \frac{1}{\cos\theta}\frac{n_2}{n_1}\frac{d_p}{2}E_{02}^{r\,2} \cdot (\exp(-\frac{2z_i}{d_p}) - \exp(-\frac{2z_f}{d_p})) \qquad (4)$$

According to eqn. (4) $d_e$ turns out to be wavelength dependent via $d_p$, see eqn. (2). As a consequence, ATR spectra of bulk media generally show increasing intensity with increasing wavelength. However, if the thickness of the layer $d = z_f - z_i$ is small compared to $d_p$ then eqn. (4) reduces to eqn (4a) which is independent of the wavelength.

$$d_e^{iso} = \frac{1}{\cos\theta}\frac{n_2}{n_1}\,d\,E_{02}^{r\,2} \qquad (4a)$$

A further case often encountered is the bulk sample extended from $z_i = 0$ to $z_f = \infty$ resulting in eqn (4b).

$$d_e^{iso} = \frac{1}{\cos\theta}\frac{n_2}{n_1}\frac{d_p}{2}\,E_{02}^{r\,2} \qquad (4b)$$

$E_{02}^{r\,2}$ denotes the square of the electric field strength in medium 2 which is proportional to the light intensity. For polarized incident light it follows

$$E_{02,||}^{r\ 2} = E_{02,x}^{r\ 2} + E_{02,z}^{r\ 2} \quad and$$
$$E_{02,\perp}^{r\ 2} = E_{02,y}^{r\ 2} \qquad (5)$$

Introducing eqn. (5) into eqn. (4) results in

$$d_{e||}^{iso} = d_{ex}^{iso} + d_{ez}^{iso} \quad and$$
$$d_{e\perp}^{iso} = d_{ey}^{iso} \qquad (6)$$

It should be concluded from eqns. (5) and (6) that straightforward application of Lambert-Beer's law to ATR spectra of isotropic samples needs measurements with either parallel or perpendicular polarized incident light. The effective thickness for unpolarized incident light $d_{e,up}^{iso}$ turns out to be a linear combination of $d_{e||}^{iso}$ and of $d_{e\perp}^{iso}$. The coefficients depend on the polarizing properties of the optical components in the spectrometer (ref. (4)) which must be determined for each instrument.

## Relative Electric Field Components

electric field components of the evanescent wave may be calculated by means of Fresnel's equations (refs. (22),(23)). For a 'nonabsorbing' thin film, e.g. a membrane assembly as depicted in Fig. 3 (medium 2), one obtains the following expressions (refs.(4), (23)):

$$E_{0x,2}^r = \frac{E_{0x,2}}{E_{0||,1}} = \frac{2\cos\theta\ (\sin^2\theta - n_{31}^2)^{1/2}}{(1-n_{31}^2)^{1/2}\ [(1+n_{31}^2)\ \sin^2\theta - n_{31}^2]^{1/2}}$$

$$E_{0z,2}^r = \frac{E_{0z,2}}{E_{0||,1}} = \frac{2\cos\theta\ \sin\theta\ n_{32}^2}{(1-n_{31}^2)^{1/2}\ [(1+n_{31}^2)\ \sin^2\theta - n_{31}^2]^{1/2}}$$

and

$$E_{0y,2}^r = \frac{E_{0y,2}}{E_{0\perp,1}} = \frac{2\cos\theta}{(1-n_{31}^2)^{1/2}} \qquad (7)$$

The meaning of $n_{ik}$ is the ratio of the refractive indices of media i and k, respectively, i.e. $n_{ik} = n_i/n_k$. According to the thin film approximation by Harrick (23) the corresponding field components of the bulk environment (medium 3) are obtained by replacing index 2 by index 3. This affects only the z-component in accordance with electrostatic boundary conditions.

For intermediate layer thickness, i.e. $d \approx d_p$ the electric field components (eqn. (7)) must be modified, either by accurate treatment of a layered system (22), or by the application of an approximation described by eqn. (8) which is based on the interpolation between the results obtained for a thin layer ($d << d_p$) and a bulk medium ($d >> d_p$) (24). The results obtained by this approximation deviate less than 5% from those got by the much more complicated accurate calculation. Eqn. (8) holds for all field components (x-, y-, and z-direction).

$$E_{02}^r(d) = E_{02}^r(thin\ layer) + (1-e^{-d/d_p})\cdot(E_{02}^r(bulk) - E_{02}^r(thin\ layer)) \qquad (8)$$

## Validity of Effective Thickness Concept

Since the effective thickness concept enables the application of Lambert-Beer's law to ATR data, experimental validation may be performed easily by comparing spectra of the same sample measured by both, ATR and transmission (T). As long as the results do not differ significantly from each other the analytical approach described above is considered to be justified. ATR and T measurements with aqueous solutions of $Na_2SO_4$ have shown that at 1 molar concentration Lambert-Beer's law is still fulfilled for the very intense $SO_4^{2-}$ stretching band at 1100 $cm^{-1}$. Even for the strong $H_2O$ bending ($\delta(H_2O)$) band of liquid water at 1640 $cm^{-1}$ the integral molar absorption coefficients determined by ATR with a germanium MIRE at an angle of incidence of $\theta = 45°$ was found to be equal to T-data within the experimental error (4). However, a few percents of deviation were found when peak values of the absorbance were used to determine the molar absorption coefficient. The latter indicates the onset of band distortion, a phenomenon well known in ATR spectroscopy under extreme conditions (23). This finding is in accordance with calculations by Harrick using Fresnel's equations with complex refractive indices (23). For Ge in contact with

liquid water and $\theta = 45°$ the analysis resulted in an upper limit of the absorption coefficient $\alpha_{max} \approx 1000\ cm^{-1}$. The concept of effective thickness as described above may be considered to be valid for $\alpha < \alpha_{max}$. For organic compounds this condition is generally fulfilled. In case of $\delta(H_2O)$ of liquid water, however, the absorption coefficient (ref. 4) results in $\alpha = \varepsilon(1640\ cm^{-1}) \cdot c = 1.82 \cdot 10^{4}\ cm^{2} \cdot mol^{-1} \cdot 5.56 \cdot 10^{-2}\ mol \cdot cm^{-3} = 1011.9\ cm^{-1}$, which indicates that the limit of validity of the approach is reached, in complete accordance with experimental data mentioned above.

## Oriented Samples

Considering a transition dipole moment $\vec{M}$ associated with a vibrational mode of a given molecule and the electric field $\vec{E}$, responsible for vibrational excitation, the intensity of light absorption depends on the mutual orientation of these vectors according to

$$\begin{aligned} \Delta I &\propto (\vec{E} \cdot \vec{M})^2 \\ &= |\vec{E}|^2 \cdot |\vec{M}|^2 \cdot \cos^2(\vec{E}, \vec{M}) \\ &= (E_x M_x + E_y M_y + E_z M_z)^2 \end{aligned} \tag{9}$$

Eqn. (9) forms the basis of orientation measurements. $M_x$, $M_y$, and $M_z$ denote the components of the transition dipole moment in the IRE fixed coordinate system shown in Fig. 4. It is usual to work with dimensionless relative intensities instead of absolute intensities in order to get rid of physical and molecular constants, e.g. the magnitude of the transition moment. Introducing the so-called dichroic ratio, the absorbance ratio obtained from spectra measured with parallel and perpendicular polarized incident light, i.e.

$$R = \frac{A_{||}}{A_{\perp}} = \frac{d_{e,||}}{d_{e,\perp}} = \frac{\int A_{||}\, d\tilde{\nu}}{\int A_{\perp}\, d\tilde{\nu}} \tag{10}$$

In order to get information on the direction of the transition dipole moment $\vec{M}$, the scalar product notation using vector components (see eqn. (9, 21)) will be used. Taking into account that in the evanescent field pp light is represented by x- and z-components, and vp light by the y-component one obtains for the dichroic ratio:

$$\begin{aligned} R &= \frac{A_{||}}{A_{\perp}} = \frac{d_{e,||}}{d_{e,\perp}} \\ &= \frac{E_x^2\, m_x^2 + E_z^2\, m_z^2 + 2\, E_x\, E_z\, m_x\, m_z}{E_y^2\, m_y^2} \end{aligned} \tag{11}$$

$m_x$, $m_y$, and $m_z$ are the unit vector components of $\vec{M}$. Eqn. (11) holds for a single crystalline sample. In a complex non crystalline molecule there are generally many possibilities of molecular arrangements, conformational changes and fluctuations. The experimentally available quantity R is therefore a ensemble mean represented by:

$$\begin{aligned} R &= \frac{A_{||}}{A_{\perp}} = \frac{d_{e,||}}{d_{e,\perp}} \\ &= \frac{E_x^2 \langle m_x^2 \rangle + E_z^2 \langle m_z^2 \rangle + 2\, E_x\, E_z \langle m_x\, m_z \rangle}{E_y^2 \langle m_y^2 \rangle} \end{aligned} \tag{12}$$

Uniaxial orientation along the z-axis is often encountered in membrane spectroscopy. In this case $\langle m_x m_z \rangle = 0$, resulting in

$$\begin{aligned} R &= \frac{A_{||}}{A_{\perp}} = \frac{d_{e,||}}{d_{e,\perp}} \\ &= \frac{E_x^2 \langle m_x^2 \rangle + E_z^2 \langle m_z^2 \rangle}{E_y^2 \langle m_y^2 \rangle} \end{aligned} \tag{13}$$

The unit vector components as presented in Fig. 4 are determined by the angles $\alpha$ and $\Phi$

$$\begin{aligned} m_x &= \sin\alpha\, \cos\Phi \\ m_y &= \sin\alpha\, \sin\Phi \\ m_z &= \cos\alpha \end{aligned}$$

*with corresponding mean squares*

$$\begin{aligned} \langle m_x^2 \rangle &= \langle \sin^2\alpha\, \cos^2\Phi \rangle = \frac{1}{2}\,(1 - \langle \cos^2\alpha \rangle) \\ \langle m_y^2 \rangle &= \langle \sin^2\alpha\, \sin^2\Phi \rangle = \frac{1}{2}\,(1 - \langle \cos^2\alpha \rangle) \\ \langle m_z^2 \rangle &= \langle \cos^2\alpha \rangle \end{aligned} \tag{14}$$

It should be noted that for an isotropic arrangement of transition moments the ensemble mean of any component of eqn. (14) result in 1/3. As a consequence eqn. (13) results in

$$R^{iso} = \frac{E_x^2 + E_z^2}{E_y^2} \tag{15}$$

which, according to eqn. (7) differs from unity. $R^{iso} = 1$ holds only for transmission spectroscopy.

Introducing eqn. (14) into eqn. (13) results in

$$R = \frac{E_x^2}{E_y^2} + 2\,\frac{E_z^2}{E_y^2}\,\frac{\langle\cos^2\alpha\rangle}{1-\langle\cos^2\alpha\rangle} \tag{16}$$

Solving eqn. (16) for $\langle\cos^2\alpha\rangle$ results in

$$\langle\cos^2\alpha\rangle = \frac{(R-\frac{E_x^2}{E_y^2})\,\frac{E_y^2}{E_z^2}}{2+(R-\frac{E_x^2}{E_y^2})\,\frac{E_y^2}{E_z^2}} \tag{17}$$

This quantity is directly related to the segmental order parameter $S_{seg}$, which corresponds to the bond order parameter encountered in nuclear magnetic resonance (NMR) spectroscopy.

$$S_{seg} = \frac{3}{2}\,\langle\cos^2\alpha\rangle - \frac{1}{2} \tag{18}$$

Perfect alignment along the z-axis would result in $\langle\cos^2\alpha\rangle = 1$, and $S_{seg} = 1$, respectively. On the other hand an isotropic arrangement of transition moments would result in the ensemble mean $\langle\cos^2\alpha\rangle = 1/3$, corresponding to $S_{seg} = 0$. Finally, isotropic arrangement of the transition moments in the x,y-plane, i.e. $\alpha = 90°$ would result in $S_{seg} = -1/2$.

Both, $\langle\cos^2\alpha\rangle$ and $S_{seg}$ are experimentally accessible by polarized light measurements.

## Effective Thickness of Oriented Samples Surface Concentration

Axial effective thickness' of isotropic samples as introduced by eqns. (4) and (6) must now be weighted by the corresponding ensemble mean of the unit vector components of the transition moment, resulting in

$$\begin{aligned} d_{ex} &= 3\langle m_x^2\rangle d_{ex}^{iso} = \frac{3}{2}\,(1-\langle\cos^2\alpha\rangle)\,d_{ex}^{iso} \\ d_{ey} &= 3\langle m_y^2\rangle d_{ey}^{iso} = \frac{3}{2}\,(1-\langle\cos^2\alpha\rangle)\,d_{ey}^{iso} \\ d_{ez} &= 3\langle m_z^2\rangle d_{ez}^{iso} = 3\,\langle\cos^2\alpha\rangle\,d_{ez}^{iso} \end{aligned} \tag{19}$$

In analogy to eqn. (6) one obtains for the effective thickness with parallel polarized incident light

$$d_{e||} = d_{ex} + d_{ez} \tag{19a}$$

$$d_{e\perp} = d_{ey} \tag{19b}$$

The surface concentration $\Gamma$ of a species in a layer of thickness d is considered as projection of the volume concentration c to the surface of the IRE. It follows from eqns. (3) and (19).

$$\begin{aligned} \Gamma = c\cdot d &= \frac{A_{||}\cdot d}{\varepsilon\cdot d_{e||}} = \frac{\int A_{||}\,d\tilde{\nu}\cdot d}{\int \varepsilon\,d\tilde{\nu}\cdot d_{e||}} \\ &= \frac{A_{\perp}\cdot d}{\varepsilon\cdot d_{e\perp}} = \frac{\int A_{\perp}\,d\tilde{\nu}\cdot d}{\int \varepsilon\,d\tilde{\nu}\cdot d_{e\perp}} \end{aligned} \tag{20}$$

$A_{||}$ and $A_{\perp}$ denote the absorbances measured with parallel and perpendicular polarized incident light, respectively. $\varepsilon$ is the molar absorption coefficient. It should be noted that eqn. (20) holds for integrated absorbance, too, provided that integrated molar absorption coefficients are used.

## SBSR SPECTROSCOPY

Most FTIR spectrometers are working in the single beam (SB) mode. As a consequence a single channel reference spectrum has to be stored for later conversion of single channel sample spectra into transmittance and absorbance spectra. This technique favors inaccuracy due to drifts resulting from the instrument or from the sample as well as disturbance by atmospheric absorptions. In order to eliminate these unwanted effects to a great extent a new ATR attachment has been constructed, converting a single beam instrument into a pseudo-double beam instrument. The

principle features of this attachment are depicted in Fig. 5.

As usually, a convergent IR beam enters the sample compartment. The focal point is now displaced by the planar mirrors M1 and M2 to the new position F, whereas the off-axis parabolic mirror M3 performs a conversion of the divergent beam into a parallel beam with fourfold reduced cross-section. This beam is focused to the entrance face of a trapezoidal IRE by a cylindrical mirror M4. Therefore, the ray propagation in the IRE is still parallel to the direction of light propagation (x-axis), enabling subdivision of the large IRE surfaces (x,y-plane) in perpendicular direction (y-axis) to the light propagation. One half of the IRE is then used for the sample (S) and the other one for the reference (R). Both, S and R, were encapsulated by flow-through cuvettes, independently accessible by liquid or gaseous flow-through. This principle is referred to as *Single Beam Sample Reference (SBSR)* technique. In a first version (refs. (3), (4)) a computer controlled chopper was used to direct the beam alternatively through the sample and reference. Later on the chopper version has been replaced by the lift version shown in Fig. 5. The cell platform is moved alternatively up and down aligning the sample and reference cuvettes with the IR beam, respectively. The lift version has two significant advantages over the chopper version (i) as it makes use of the full beam of the spectrometer resulting in twice the single channel energy of the chopper version, and (ii) still more relevant for most applications, it compensates the inhomogeneous light flux inherent in most IR spectroscopic instruments.

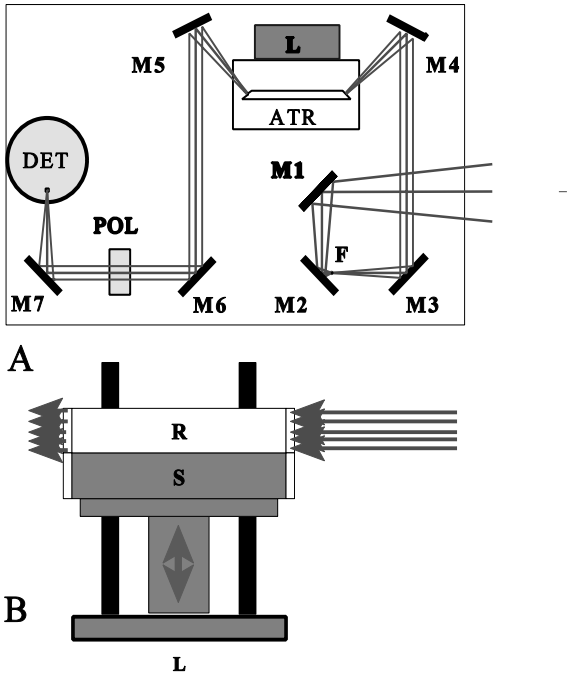


**FIGURE 5.** Single Beam Sample Reference (SBSR) ATR attachment. (A) The focus in the sample compartment is displaced to the position F by the planar mirrors M1 and M2. The off-axis parabolic mirror M3 produces a parallel beam with a diameter of one centimeter, i.e. half of the height of the IRE. The cylindrical mirror M4 focuses the light to the entrance face of the IRE. M5 which has the same shape as M4 reconverts to parallel light passing via the planar mirror M6 through the polarizer POL and being focused to the detector DET by the off-axis parabolic mirror M7. (B) Alternative change from sample to reference and vice versa is performed by computer controlled lifting and lowering of the ATR cell body.

Thus SBSR absorbance spectra are calculated from sample and reference single channel spectra which have been measured with very short mutual time delay. Fig. 6 shows the results of a series of HD exchange measurements performed in the SBSR mode with the enzyme creatine kinase (CK). The enzyme was adsorbed from $H_2O$ buffer to a DPPA/CL supported bilayer as described in ref. (16).

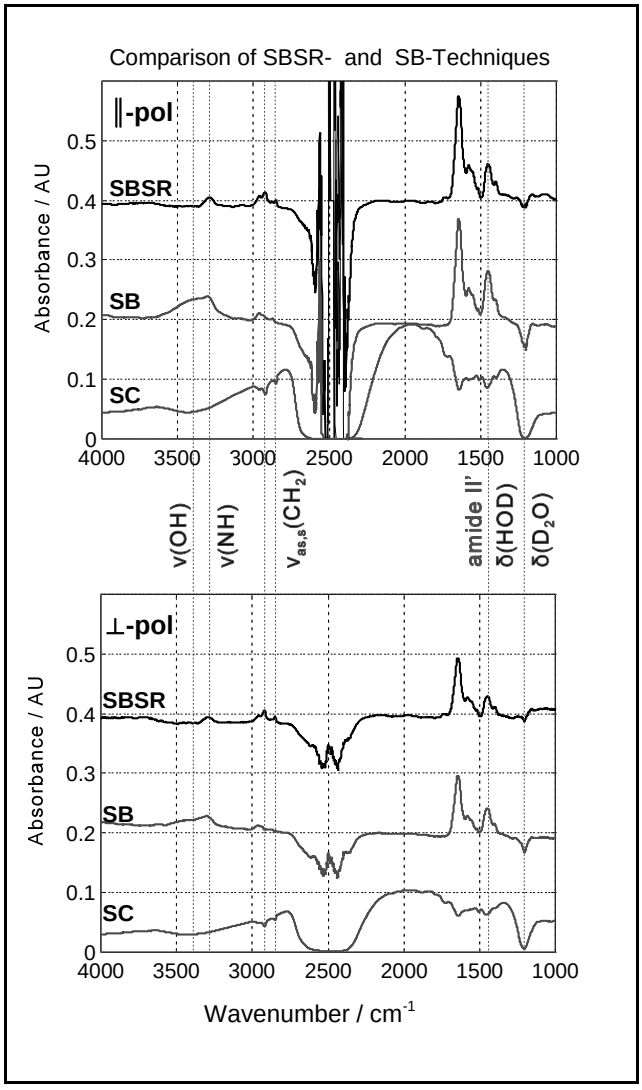


**FIGURE 6.** Comparison of Single Beam Sample Reference (SBSR) pseudo-double beam technique with conventional single beam (SB) technique. Very low energy in the 2500 $cm^{-1}$ and 1200 $cm^{-1}$ region resulted from stretching $\nu(D_2O)$ and bending $\delta(D_2O)$ absorptions of liquid $D_2O$, respectively, as shown by a single

channel (SC) spectrum. The supported bilayers in the sample and reference cuvettes consisted of a dipalmitoylphosphatidic acid (DPPA) LB monolayer and a cardiolipin (CL) adsorbed monolayer. Both membranes exhibited the same age, since the LB layer covered the whole width of the IRE, and CL adsorption from vesicles occurred synchronously by two independent equal circuits. In a second step creatine kinase (CK) was adsorbed from a circulating solution in the sample channel, ref. (16). Therefore, the absorbance spectra shown in this figure reflect adsorbed CK as well as any other differences between S and R channel. Obviously, there are more detectable differences in the SB mode than in the SBSR mode, because SBSR reflects the actual difference between S and R, while SB shows the difference between the actual sample spectrum and a stored (older) reference spectrum. In this case, the partly different results obtained in the SBSR and SB mode result predominately from a slow uptake of $H_2O$ vapor by the circulating $D_2O$ solutions. This leads to overlapping of ν(NH) and amide II' of CK, as well as an overcompensation of $D_2O$ absorption bands (~ 2500 $cm^{-1}$ and 1200 $cm^{-1}$). It should be noted that the slight overcompensation of $\delta(D_2O)$ at 1200 $cm^{-1}$ is significant, since it reflects the reduced water content in the sample cuvette due to displacement by the CK layer. pp and vp absorbances are in accordance with eqns. (3) and (4), using $z_i$ = 50 Å, $z_f$ = 143 Å, $\varepsilon(\delta(D_2O)) = 1.38 \cdot 10^4$ $cm^2 \cdot mol^{-1}$. Ge IRE, angle of incidence, θ = 51°, number of active internal reflections, N = 36.7. The refractive indices were: $n_1$ = 4.0, $n_2$ = 1.45, and $n_3$ = 1.30, see Fig. 3.

The conventional SB spectrum reflects the whole history of the sample, whereas the SBSR spectrum reflects the sample state when compared with a reference of the same age. Therefore, the SB spectrum contains the HDO produced by slight $H_2O$ contamination during the experiment in addition to the spectrum of CK. The former obscures the shape of ν(NH) and amide II' bands, which is an obvious disadvantage of the SB mode.

For HD exchange a $D_2O$ buffer solution was circulated through the sample and reference cuvette of the ATR cell during three days. As a consequence slight contamination of $D_2O$ by atmospheric $H_2O$ could not be avoided in the course of this long-time experiment. The resulting HDO gave rise to absorption bands near 3400 $cm^{-1}$ and near 1450 $cm^{-1}$ interfering with NH stretching (ν(NH)) of non-exchanged amide protons, and with amid II' of deuterated amide groups of the protein, respectively. Since in sample and reference contamination by hydrogen is approximately the same due to equal treatment of the circulating $D_2O$ buffer solutions, the HDO absorption bands (ν(OH) and δ(HDO)) will be compensated to a major extent, as demonstrated by Fig. 6, trace SBSR. The SBSR trace represents predominately membrane bound CK in a partially deuterated state. The sample consisted of a DPPA/CL/CK assembly, and the reference of a DPPA/CL supported bilayer. Since a sequence of SBSR spectra consists of two independent sequences of single channel spectra, the collected data may by analyzed in the SB mode as well. Doing this by using the single channel spectrum of the sample channel measured in the SBSR mode before CK adsorption (DPPA/CL in $D_2O$ environment in S and R) as reference and a corresponding single channel spectrum after about 12 hours of CK exposure to $D_2O$ buffer as single channel sample spectrum. The resulting SB absorbance spectrum is also presented in Fig. 6, trace SB. Thus SBSR and SB spectra shown in Fig. 6 had exactly the same experimental conditions. To make best use of SBSR data, it is recommended to analyze the data by both modes, SBSR and SB since an unwanted synchronous breakdown of sample and reference assembly, e.g. by hydrolysis of a polymer matrix existing in S- and R-channel, or by equal loss of lipid molecules from a supported bilayer, would be obscured in the SBSR mode, but unambiguously detected in the SB mode.

## LOCAL ANESTHETIC MEMBRANE INTERACTION

The mechanism of action of local anesthetics (LA) is still subject to discussion among biophysicists, physicians, and pharmacists, although the teaching opinion, generally accepted among physicians, claims that tertiary amine LA's will react specifically from the interior of the cell with a receptor in the sodium channel (25). This reaction is suggested to block the sodium influx, thus interrupting nerve signal transmission. Of course, FTIR studies with model membranes can't validate or reject the suggestion of a specific action of LA's. However, significant information on the interaction with lipid bilayers is available with respect to partition coefficient, degree of protonation of bound LA, and influence on structural changes of the lipid bilayer and LA upon binding.

Dibucaine (DIBU) or cinchocaine which is a synonym of DIBU was used as a model LA. Its chemical formula is depicted in Fig. 7. DIBU has a $pK_a$ value of 8.87 in solution. 99.9 % of the molecules in the bulk solution are in the protonated state at pH 5.5 (Fig. 7).

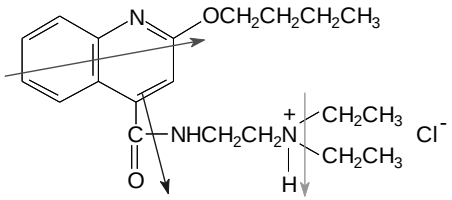


**FIGURE 7.** Structure of the local anesthetic dibucaine (DIBU). The arrows denote the approximate directions of the transition moments of the aromatic ring stretching at 1407 $cm^{-1}$, the C=O double bond stretching band at 1670 $cm^{-1}$, and the $N^+$-H stretching band at 2700 $cm^{-1}$.

NMR studies have been performed at this low pH in order to make sure that membrane bound DIBU is also in the protonated state.This would facilitate the interpretation of spectra (26). For the sake of comparison our experiments have been performed under the same conditions. The model membrane consisted of a DPPA/POPC supported bilayer. A

series of DIBU concentrations (0.5 mM to 10.0 mM) were prepared in 20 mM phosphate-borate-citrate buffer (pH 5.5) containing 100 mM sodium chloride. The solutions were pumped in a closed cycle through the ATR cuvette (Fig. 2) while ATR spectra were measured at the same time.

Typical polarized absorbance spectra of the membrane interacting with a 10 mM DIBU solution are shown in Fig. 8 trace a. Trace b was obtained from the spectra of a 100 mM solution of DIBU by scaling down with a factor 0.299 for parallel polarization (pp, $||$) and 0.325 for perpendicular polarization (vp, $\perp$). The aromatic ring stretching vibration at 1407 $cm^{-1}$ was used for scaling, because this band turned out to be insensitive to pH changes. Since the scaling factors were larger than 0.1, there is unambiguous evidence for LA adsorption to the lipid membrane. Moreover, different scaling factors point to a certain ordering of DIBU upon membrane binding.

## Structural Changes upon LA Binding

The most prominent spectral changes result from the DPPA/POPC bilayer. First, the negative absorbance at 1740 $cm^{-1}$ resulting from the ester C=O stretching vibrations should be mentioned. At first sight, loss of lipid molecules due to LA interaction could be supposed. Watching closer, however, reveals that in such a case even more negative bands should be expected at the wavenumbers of the more intense $>PO_2^{2-}$ stretching bands at 1230 $cm^{-1}$ and 1090 $cm^{-1}$. Since there is no evidence for such negative $>PO_2^{2-}$ stretching bands, one may exclude lipid loss upon LA binding. This conclusion is supported by the observation that the original spectrum of the bilayer is restored after washing out of DIBU. A reasonable explanation for the behavior of the ν(C=O) band is a conformational change of one or both fatty acid ester groups induced by LA interaction. This might induce a change of the composition of the corresponding normal mode. As a consequence the associated transition moment $\vec{M}$ (see Fig. 4) must be expected to be changed, too, which according to eqns. (3) and (9) would also influence the magnitude of the molar absorption coefficient ε. In case of ν(C=O) a decrease of ε is expected. Conformational change of the hydrocarbon chain region is indicated by the symmetric and antisymmetric $CH_2$ stretching bands at 2850 $cm^{-1}$ and 2920 $cm^{-1}$, respectively. For a perfectly aligned hydrocarbon chain along the z-axis the mean transition moments of both, $\nu_s(CH_2)$ and $\nu_{as}(CH_2)$ are expected to be in the x,y-plane (see Fig. 4), i.e. perpendicular to the z-axis and isotropically distributed around this axis. Since in this case $\langle \cos^2 \alpha \rangle = 0$, it follows from eqn. (19) that $d_{e\perp} = d_{ey} = 1.5\ d_{ey}^{iso}$ is decreased to $d_{ey} = d_{ey}^{iso}$ upon conversion to random conformations. In case of parallel polarized incident light one obtains from eqns. (19) and (19a) $d_{e||} = 1.5\ d_{ex}^{iso}$ for perfect chain alignment along the z-axis. Conversion to random structures increases the effective thickness to $d_{e||} = d_{ex}^{iso} + d_{ez}^{iso}$.

Under the given conditions one obtains for a supported bilayer of thickness d = 50 Å (θ = 45°, $n_1 = 4.0$, $n_2 = 1.45$, $n_3$ (2900 $cm^{-1}$) ≈ 1.40 (anomalous dispersion of $H_2O$)) the axial effective thickness' $d_{ex}^{iso} = 50$ Å, $d_{ey}^{iso} = 58$ Å and $d_{ez}^{iso} = 58$ Å. As a consequence the dichroic response to the above mentioned perturbation of hydrocarbon chain ordering will be:

$d_{e||} = 75$ Å ⇒ $d_{e||}^{iso} = 108$ Å, and $d_{e\perp} = 88$ Å ⇒ $d_{e\perp}^{iso} = 58$ Å thus confirming qualitatively the absorbance decrease in the vp-spectrum and the synchronous increase in the pp-spectrum as a consequence of chain disordering (Fig. 8).

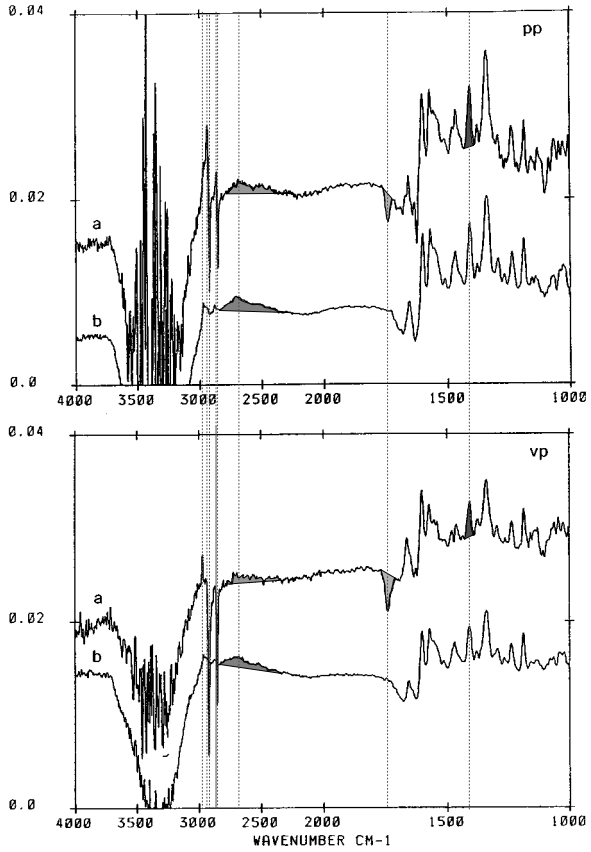


**FIGURE 8**. SBSR ATR IR spectra of the local anesthetic dibucaine (DIBU). **a:** 10 mM DIBU in contact with a DPPA/POPC supported bilayer. **b:** 100 mM DIBU in direct contact with the IRE, scaled down by 0.299 (pp), and 0.325 (vp). 100 mM NaCl, 20 mM BPC buffer pH 5.5. Parallel (pp) and perpendicular (vp) polarized incident light at θ=45°. Germanium (Ge) IRE, N=19.3 active internal reflections. The reference cuvette contained a DPPA/POPC membrane under the same conditions.

It should be noted that orientational changes of the fatty acid ester groups most probably contribute also to the absorbance of ν(C=O), however, the effect by the expected decrease of ε should be dominant, since negative bandes are observed in both polarizations. On the other hand, a decrease of ε(ν($CH_2$)) should also be taken into account upon conformational changes of the hydrocarbon chain (27).

A quantitative analysis of hydrocarbon chain ordering

based on polarized IR ATR spectra and on intensity considerations will be given in ref. (9). The qualitative interpretation of chain order decrease due to LA interaction as given above is strongly supported by a shift of both, $\nu_s(CH_2)$ and $\nu_{as}(CH_2)$ to higher wavenumbers paralleled by a decrease of peak absorbances. This effect is indicative for hydrocarbon chain disordering (28). Finally the behavior of the antisymmetric methyl stretching vibration at 2963 $cm^{-1}$ should be mentioned. In contrast to the $CH_2$ stretching bands, this band shows an increase in the vp spectrum upon LA interaction. In the pp spectrum, it is only visible as a shoulder. Qualitatively, one has to conclude, that the transition moment of this band ($\nu_{as}(CH_3)$) exhibits a predominant interaction with $E_z$ in the unperturbed state. Reducing the ordering by LA interaction lead to enhanced interaction with $E_y$, i.e. increasing absorbance in the vp spectrum.

Unambiguously, DIBU interaction with a DPPA/POPC bilayer lead to a significant hydrocarbon chain disordering. As a consequence local anaesthesia might result only from a disturbance of the global membrane structure which could idirectly influence the structure and function of proteins relevant for nerve signal transduction.

Finally, it should be noted, that the original ordering of the supported bilayer was restored, when the LA was detached by circulating pure buffer solution through the ATR cuvette.

## Apparent $pK_a$ of Bound DIBU and Partition Coefficient

Several absorption bands in the 1000 - 1800 $cm^{-1}$ region are changing shape and wavenumber upon DIBU interaction. A discussion of some bands reflecting conformational and pH induced changes of DIBU as well as of phospholipids will be given in ref. (9).

Two absorption bands, however, are of special interest in connection with the determination of the degree of protonation of bound DIBU ($DIBU^+$) as well as of the partition coefficients $K_p$ of DIBU, $DIBU^+$ and $DIBU_{tot}$. The aromatic ring stretching vibration $\nu$(C=C) at 1407 $cm^{-1}$ has turned out to be insensitive to pH changes, therefore it can be used to determine the total amount of bound DIBU ($\Gamma(DIBU_{tot})$). On the other hand, the $N^+$-H stretching vibration $\nu(N^+H)$ at 2700 $cm^{-1}$ gives direct information on the amount of bound $DIBU^+$ ($\Gamma(DIBU^+)$).

The surface concentration of deprotonated DIBU is obtained by the difference $\Gamma(DIBU) = \Gamma(DIBU_{tot}) - \Gamma(DIBU^+)$. The result of a quantitative analysis of an experimental series with measurements at variable bulk DIBU concentration is presented in Fig. 9.

Before going into details, a short explanation shall be given, on how adsorption isotherms are obtained from FTIR ATR raw data. 20 - 40 internal reflections are optimum for *in situ* mono- or submonolayer spectroscopy in aqueous environment when using a germanium IRE with an angle of incidence of $\theta \approx 45°$ (4). Under these conditions, intense bands of dissolved organic compounds become visible in the spectrum at bulk concentrations above about 0.5 mM.

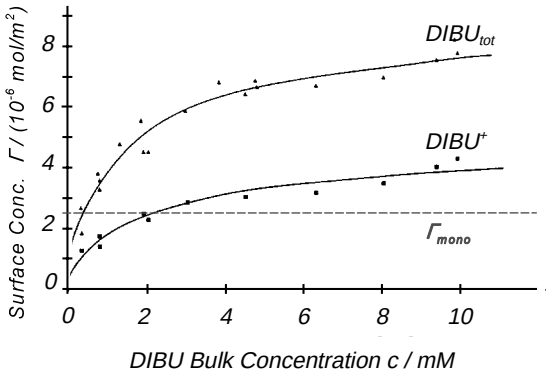


**FIGURE 9.** Surface concentration of dibucaine (DIBU) determined by means of eqn. (20) as a function of bulk concentration c at bulk pH 5.5. $DIBU_{tot}$: Adsorption isotherm of total amount of membrane bound DIBU. $DIBU^+$: Adsorption isotherm of protonated fraction of membrane bound DIBU. Both adsorption isotherms may be described by the Langmuir model resulting in $\Gamma_{max}(DIBU_{tot}) = 8.22 \cdot 10^{-6}$ mol/m², and $\Gamma_{max}(DIBU^+) = 3.88 \cdot 10^{-6}$ mol/m². On the other hand, $\Gamma_{mono} = 2.5 \cdot 10^{-6}$ mol/m² denotes the calculated surface concentration of a packed monolayer of DIBU from the molecular cross section of 68 Å², ref. (26). Mean monolayer coverage is already achieved near 1 mM bulk concentration. A possible explanation of the apparent discrepancy with fits according to the Langmuir model is adsorption of preformed DIBU aggregates from bulk solution to the membrane. Membrane bound DIBU consists of about equal amounts of the protonated and deprotonated form.

Therefore, in the first step of the analysis, the polarized absorbance spectra have to be corrected for bulk DIBU absorption using eqns. (2 - 4) and eqn. (7). For a bulk medium, index 2 in eqn. (7) must be replaced by index 3 (see text). The following values have been used for calculation: $n_1 = 4.0$, $n_2 = 1.45$ (membrane + DIBU), $n_3 = 1.31$ ($H_2O$, 1407 $cm^{-1}$), $\theta = 45°$, $\lambda = 7.11 \cdot 10^{-4}$ cm ( 1407 $cm^{-1}$), $\varepsilon(1407\ cm^{-1}) = 1.80 \cdot 10^5$ cm²/mol, $z_1 = 5.0 \cdot 10^{-7}$ cm, $z_f = \infty$, N = 19.3 (number of active internal reflections). Under these conditions, a 10 mM bulk DIBU solution results in at 1407 $cm^{-1}$: $A_{||}(DIBU) = 2.52$ mAU, and $A_{\perp}(DIBU) = 1.26$ mAU, respectively. For correction of bulk absorption one may subtract the corresponding DIBU spectrum measured without membrane, since according to eqn. (4) there is an attenuation of only about 1% due to the displacement of the solution by the supported membrane of thickness d = 50 Å. The remaining spectrum reflects bound DIBU and conformational changes of the lipid bilayer induced by DIBU interaction. Since most

supported membrane assemblies feature uniaxial partial orientation along the membrane normal (z-axis) quantitative analysis must be based on eqns. (17), (19) and (20). The following dichroic ratios were determined from Fig. 8: R(1407 $cm^{-1}$) = 1.60, and R(2700 $cm^{-1}$) = 1.42. The former value is very close to that of an isotropic layer which is according to eqn. (15) $R^{iso}$ = 1.61, however, since the dichroic ratio of the $\nu(N^+H)$ band deviates significantly from $R^{iso}$ one may conclude that DIBU is not randomly adsorbed to the lipid bilayer but exhibits some ordering. As a consequence, the transition moment $\nu_{ar}$(C=C) at 1407 $cm^{-1}$ is expected to have a mean incline of about 55° (magic angle) with respect to the z-axis.

At first sight Fig. 9 reveals that despite of the low bulk pH of 5.5 membrane bound $DIBU_{tot}$ behaves stoichiometrically like a 1:1 complex of protonated $DIBU^+$ and deprotonated DIBU species. At low bulk concentrations one could argue for DIBU being dissolved in the hydrophobic region of the membrane, and $DIBU^+$ being located at the membrane surface. DIBU penetrating into the lipid phase would explain the significant disturbance of hydrocarbon chain ordering discussed above. This interpretation may be correct, however, it can't explain the nearly constant ratio of stoichiometric coefficients up to bulk concentrations of 10 mM because already below 1 mM bulk DIBU concentration bound $DIBU_{tot}$ exceeds the quantity required for a monomolecular coverage of the membrane surface (DIBU cross-section 68 $Å^2$, ref. (26)). It is known from earlier work (7) that LA's tend to multilayered adsorption at elevated bulk concentration. Vapor pressure osmometry has revealed that LA form aggregates already in bulk solution (8), which could explain the significantly higher DIBU surface concentrations obtained by fitting experimental data according to the Langmuir isotherm, see Fig. 9. In view of these findings we suggest that the observed stoichiometric ratio DIBU : $DIBU^+$ = 1 : 1 is characteristic of associated DIBU, at least above 1 mM bulk concentration. DIBU multilayer formation at the membrane surface is also supported by the observation that the mean order parameter of the $CH_2$ groups of hydrocarbon chains of POPC as determined by eqns. (17) and (18) is found to decrease from $S_{mean}$(c=0 mM) = 0.65 in the pure DPPA/POPC supported membrane to $S_{mean}$(c≥3mM) = 0.20. Thus hydrocarbon chain ordering was no longer affected by DIBU adsorption above 3 mM bulk DIBU concentration, refs. (8) and (9).

In view of these facts, the use of a partition coefficient is only meaningful for the limiting case c ⇒ 0 mM. Denoting bulk DIBU concentration by c and the concentration of DIBU in the membrane by $c_m$ one obtains for the partition coefficient under consideration of eqn. (20)

$$K_p = \lim_{c \to 0} \frac{c_m}{c} = \frac{\Gamma}{d \cdot c} \qquad (21)$$

Taking the experimental data from Fig. 9 to calculate the limits according to eqn. (21) one obtains $K_p(DIBU_{tot})$ = 1410, $K_p(DIBU^+)$ = 668, and $K_p(DIBU)$ = $9.2 \cdot 10^5$, respectively. For details, the reader is referred to refs. (8) and (9).

## TIME RESOLVED MODULATED EXCITATION (ME) SPECTROSCOPY

### External ME of Lipids, Peptides and Proteins

Change of any external thermodynamic parameter generally excerts a specific influence on the state of a system. The sytem response will be a relaxation from the original state (e.g. an equilibrium) to a new equilibrium state. In case of a periodic change (modulation) of the parameter, the system response will also be periodic, i.e. those absorption bands of the spectrum which result from stimulated molecules or parts of them will be labelled by the same frequency. As a consequence, it will be possible to separate the modulated response of the system, which is correlated with the external stimulation from the stationary response, resulting from parts of the system that were not affected by modulated excitation (ME) and from the background. Moreover, if the kinetics of the stimulated process is in the same time range as the period of external stimulation, phase-lag and amplitude measurements of modulated absorbances give information on the reaction scheme and the kinetics of the stimulated process. Hydration modulation, e.g. was applied to determine the hydration sites of lecithins (29), (30).

Temperature ME of poly-L-lysine was used to study induced periodic secondary structural changes as well as the sequence of transients (20). The classical ATR set-up (see Fig. 2 facilitates the application of electric fields to membrane assemblies, since a Ge ATR plate, supporting the membrane, may be used as one electrode, and the back-wall of the cuvette as counter electrode. First use of electric field ME of immobilized acetyl choline esterase (AChE) was reported in ref. (31). In the view of to-day, the interpretation of a field-dissociation effect (second Wien effect) of carboxylic acid residues of AChE must be qualified. Since Ge decomposes at slightly positive potentials, forming germinic acid, the periodic deprotonation and reprotonation of -COOH groups of AChE may be interpreted as a superposition of electric field and pH-effect. As a consequence, passivation of the Ge surfaces (32) is a prerequisite for electric field ME experiments. The problem of anodic decomposition of germanium does not exist in the case of electric field ME of liquid crystals (33), (34).

Electronic ME of photochemical processes by modulated UV-/VIS-light enables access to a wide range of excitation frequencies. Light flux modulation in the kHz range, which

may be easily performed by means of a mechanical chopper, enables kinetic analysis even in the µs region as shown in the case of the photooxidation of pyrocatechol by modulated electronic excitation IR and ESR spectroscopy (35).

## Schematic Set-up for ME Spectroscopy

The principle set up for a modulated excitation (ME) experiment is depicted by Fig. 10. In contrast to relaxation experiments where step-excitation (SE) is used ME technique is based on a periodic stimulation. Both techniques give access to the characteristic dynamic quantities of a system, the relaxation constants. The response of SE is a superposition of exponentials, $\exp(-t/\tau_i)$, where $\tau_i$ denotes the i-th relaxation time of the system. ME on the other hand results in a superposition of sine waves, $\sin(\omega t+\phi_i)$ where the phase lag $\phi_i$ is given by $\phi_i=\arctan(-\omega\tau_i)$, see eqn. (28).

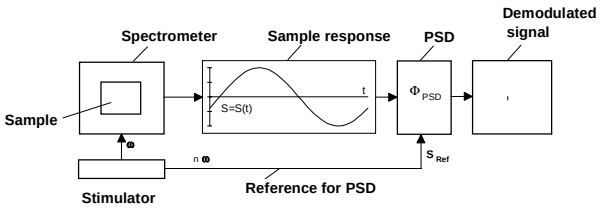


**FIGURE 10.** Schematic set up for modulated excitation (ME) experiments. A periodic excitation is exerted on the sample with frequency ω. The sample response as sensed e.g. by IR radiation contains the frequency ω at the wavelength's that are significant for those parts of the sample that have been affected by the stimulation. Selective detection of the periodic sample responses is enabled by phase sensitive detection (PSD), resulting in the amplitudes $A_n$ of the fundamentals ω and the harmonics nω (n=2, 3, ....) as well as the phase shifts $\phi_n$ between the n-th harmonic and the stimulation. This phase shift is indicative of the kinetics of the stimulated process and of the underlaying chemical reaction scheme.

## Temperature Modulated Excitation (T-ME) of Chemical Reactions

The principles of T-ME may be elucidated by considering the simple reversible chemical reaction between two species $A_1$ and $A_2$ where $k_{12}$ and $k_{21}$ denote the rate constants of forwards and backwards reaction.

$$A_1 \underset{k_{21}}{\overset{k_{12}}{\rightleftharpoons}} A_2$$

If the sample is exposed to a periodic temperature stimulation according to

$$T(t)=T_i+\frac{\Delta T}{2}(1-\cos\ \omega t) \tag{22}$$

where $T_i$, $\Delta T$ and ω denote the initial temperature, the peak to peak temperature variation and the angular frequency, respectively. The influence of temperature on rate constants may be described by the Arrhenius equation. Since $\Delta T$ is small ($\leq$ 5°C), the linearized form will be used in this context, leading to

$$\begin{aligned} k_{ik}(t) &= k_{ik}(\overline{T})+\frac{\Delta k_{ik}}{2}(1-\cos\omega t) \\ with \quad \Delta k_{ik} &= k_{ik}(T_i)\frac{E_{ik}}{RT_i^2}\Delta T \end{aligned} \tag{23}$$

$k_{ik}$ denotes the rate constant from species i to species k and $E_{ik}$ is the corresponding activation energy.

Introducing the reaction number ξ as the relevant concentration parameter for turnover description

$$[A_1]=[A_1]_0-\xi, \quad [A_2]=[A_2]_0+\xi \tag{24}$$

and introducing eqn. (24) into the rate equations for $A_1$ and $A_2$ results in the rate equation for ξ

$$\begin{aligned} \dot{\xi} = & \\ & -(\overline{k}_{12}+\overline{k}_{21}-\frac{1}{2}(\Delta k_{12}+\Delta k_{21})\cos\omega t)\cdot\xi \\ & -\frac{1}{2}(\Delta k_{12}[A_1]_0-\Delta k_{21}[A_2]_0)\cos\omega t \\ & +\ \overline{k}_{12}[A_1]_0-\overline{k}_{21}[A_2]_0 \end{aligned} \tag{25}$$

Since the peak to peak variation of the rate constants $\Delta k_{12}$ and $\Delta k_{21}$ are small compared to the mean values $\overline{k}_{12}$ and $\overline{k}_{21}$, the third term in paranthesis of the coefficient of ξ in eqn. (25) may be neglected. The solution of the differential equation with constant coefficients is then given by eqn. (26) which describes the response of the reaction number. Insertion of eqn. (26) into eqn. (24) results in the time dependent behavior of the concentrations of species $A_1$ and $A_2$. It contains the relaxation from the initial state to the steady state which is reached for $t\geq 3\tau$, where τ denotes the relaxation time. In this simplest case of a reversible reaction τ is the inverse of the sum of the two rate constants, i.e. $\tau=(k_{12}+k_{21})^{-1}$. Modulation experiments are generally started after an initial period of 3τ where relaxation is completed to

about 95%. The relevant steady state solution is then given by eqn. (27).

It should be noted that the quantity ($k_{12}$+$k_{21}$) appears as inverse relaxation time τ in the exponentials of the general solution as well as in amplitude and phase angle of the steady state solution eqns. (27) and (28). This fact proves the equivalence of relaxation and modulation techniques.

$$\xi(t) = \frac{\bar{k}_{12}[A_1]_0 - \bar{k}_{21}[A_2]_0}{\bar{k}_{12} + \bar{k}_{21}} \left(1 - \exp(-(\bar{k}_{12} + \bar{k}_{21})t)\right)$$

$$+ \frac{(\bar{k}_{12} + \bar{k}_{21})(\Delta k_{12}[A_1]_0 - \Delta k_{21}[A_2]_0)}{2((\bar{k}_{12} + \bar{k}_{21})^2 + \omega^2)} \exp(-(\bar{k}_{12} + \bar{k}_{21})t)$$

$$- \frac{1}{2}(\Delta k_{12}[A_1]_0 - \Delta k_{21}[A_2]_0) \sqrt{\frac{1}{1 + (\frac{\omega}{\bar{k}_{12} + \bar{k}_{21}})^2}} \cos(\omega t + \phi)$$

(26)

For t→∞ one obtains the stationary solution

$$\xi(t) = -\frac{1}{2} \frac{\bar{k}_{12}[A_1]_0 - \bar{k}_{21}[A_2]_0}{\bar{k}_{12} + \bar{k}_{21}} \cdot$$

$$\sqrt{\frac{(\Delta k_{12}[A_1]_0 - \Delta k_{21}[A_2]_0)^2}{1 + (\frac{\omega}{\bar{k}_{12} + \bar{k}_{21}})^2}} \cos(\omega t + \phi)$$

(27)

with

$$\phi = \arctan(-\frac{\omega}{\bar{k}_{12} + \bar{k}_{21}}) = \arctan(-\omega\tau)$$

(28)

It follows from eqns. (27) and (28) that the product ωτ is the relevant kinetic parameter in ME spectroscopy. For ω→0 the system is expected to be able to respond immediately to the external stimulation. ωτ=1 results in an amplitude damping by a factor of $\sqrt{2}$ (3 dB point), paralleled by a phase shift of ϕ=-45°, whereas for ω→∞ the amplitude approachs zero and the phase angle ϕ=-90°. Consequently, the simple chemical reaction under consideration behaves just like an electronic RC low pass filter.

Of course, the amplitude and phase dependence on modulation frequency becomes more complex for more complicated chemical reaction schemes, however, any scheme features a characteristic amplitude/phase-frequency dependence. As soon as phase resolved ME experiments at different modulation frequencies are available, ME technique will enable a more detailed kinetic analysis of the system then SE technique (relaxation technique) because of the additional experimental degree of freedom given by the modulation frequency ω.

**T-ME of the α Helix to β Pleated Sheet Conversion of Poly-L-Lysine**

A poly-(L)-lysine (PLL) film cast on an ATR plate and hydrated with $D_2O$ (80% rel. humidity, 28°C) was exposed to a periodic temperature variation of ΔT/2=±2°C at the mean value of $\bar{T}$ = 28°C. The results obtained after phase sensitive detection (PSD) are shown in Fig.11. Part (A) shows the stationary spectrum and part (B) phase resolved spectra of the system response with the fundamental frequency ω. The numbers indicated on the spectra denote phase difference between the modulated excitation and phase setting at the phase sensitive detector (PSD). The ME spectra shown in Fig. 11B may be expressed by eqn. (29)[19, 20].

$$\Delta A(\tilde{\nu}, \phi_{PSD}) = \kappa \cdot \sum_{i=1}^{N} \Delta A_{0i}(\tilde{\nu}) \cos(\phi_i - \phi_{PSD})$$

(29)

$\Delta A_{0i}(\tilde{\nu})$ is the i-th component-spectrum in which each band has the same phase angle $\phi_i$. Consequently, this set of bands may be considered to be correlated, i.e. to belong to a population of molecules or functional groups featuring the same kinetic response to the external stimulation. In such a population all absorbance bands exhibit a periodic dependence on the PSD phase setting $\phi_{PSD}$. The amplitudes become maximum for $(\phi_i - \phi_{PSD}) = 0^\circ$, minimum (negative) for $(\phi_i - \phi_{PSD}) = 180^\circ$, and zero for $(\phi_i - \phi_{PSD}) = 90^\circ$ *or* $270^\circ$. Obviously, $\phi_{PSD}$ can be used to sense the phase angle $\phi_i$ of a population of absorption bands, because $\phi_{PSD}$ is a parameter under experimental control. The most accurate determination of $\phi_i$ is got by performing a line shape analysis of the phase resolved spectra shown in Fig. 11B, followed by fitting each component according to eqn. (29), see ref. 20.

The first impression on comparing Fig. 11A with Fig. 11B is that modulation spectra are significantly better resolved. The spectral resolution was 4 $cm^{-1}$ for both, stationary and modulation spectra. However, overlap is drastically reduced in the latter, because they contain only anbsorption bands from species that have been affected by the external stimulation. Furthermore, Fig. 11B shows that not only the intensity but also the shape of phase-resolved spectra is changing with $\phi_{PSD}$-setting. This is an unambiguous indication of the existance of populations of conformational states featuring different phase angles $\phi_i$. Extraction of these populations according to eqn. (29) enabled the assignment of

transient species in the amide I' and amide II' regions. For details the reader is referrred to ref. (20). Attention should be drawn to a correlation between $CH_2$ stretching and the secondary structure of PLL which which has not been reported so far. The weak absorption bands at 2865 $cm^{-1}$ and 2935 $cm^{-1}$ result from symmetric and antisymmetric stretching of the $CH_2$ groups of the lysine side chains. They displaced by appproximately 3 $cm^{-1}$ towards lower wavenumbers with respect to the corresponding bands in the stationary state (Fig. 11A). This finding is indicative for a conformational change of a hydrocarbon chain from gauche defects into trans conformations (28). Since these

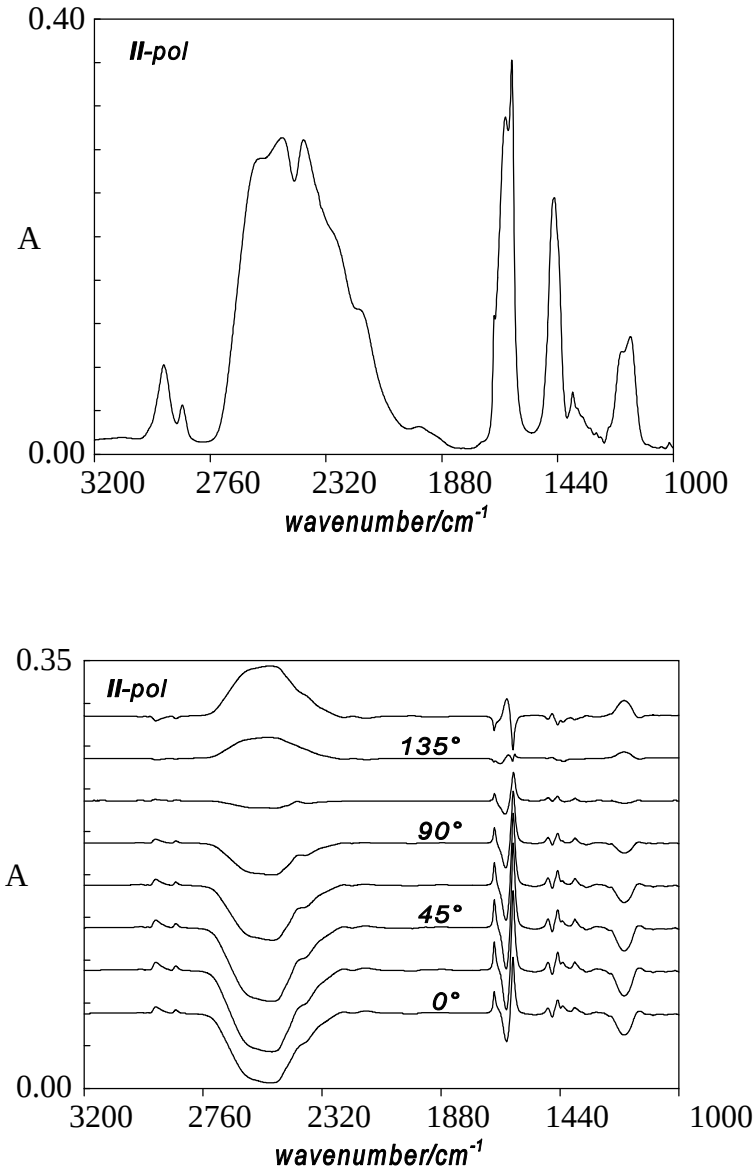


**FIGURE 11.** Parallel polarized T-ME FTIR spectra of a poly-(L)-lysine deuterobromide film hydrated with $D_2O$ (80% rel. hum., 28°C). The film was deposited on a CdTe ATR plate. A rectangular temperature stimulation was applied with a period of 14.7 min ($\omega$=0.427 $min^{-1}$) at $\bar{T}$ =28°C ± 2°C. Angle of incidence: $\theta$ = 45°, mean number of internal reflections: N=9-10. (A) Stationary part of the T-MEIR spectrum of PLL. (B) Set of phase-resolved T-MEIR spectra after phase sensitive detection (PSD) at phase settings $\phi_{PSD}$ = 0°-157.5° (phase resolution 22.5°) with respect to the T-stimulation. $\phi_{PSD}$ = 0° means in-phase with temperature switching from 26°C to 30°C. Heat transfer from the thermostats to the sample resulted in an additional phase lag of $\phi_T$ = 25°. (From ref. 20).

bands are correlated with the formation of antiparallel β-pleated sheet structure (amide I' bands at 1614 $cm^{-1}$ and 1685 $cm^{-1}$). We conclude therefore, that the conversion of PLL from α helix to β sheet is paralleled by a conformational change of the side chain from a bent to a extended structure.

**T-ME of Reversible Unfolding/Folding of RNase A**

Understanding of the molecular mechanism of protein folding and unfolding is of increasing interest not least because of molecular biological approaches to protein synthesis and modifications. RNase A is an enzyme that may be unfolded/denatured by heating and refolded/renatured upon cooling. Kinetic FTIR measurements have been reported recently using temperature jump techniques (21), (36). In this article we report the first preliminary T-ME experiments performed in solution. The stimulation amplitude was $\Delta T/2 = 5°C$ at $\overline{T} = 64°C$ with a period of $\tau_m = 25$ s. A sequence of time resolved spectra is shown in Fig. 12. Like in case of PLL there are drastic diffrences between the modulation spectra and the stationary spectrum (upper trace). As mentioned above modulation spectra suppress any absorbance which is not labelled by the stimulation frequency. Two interesting observations should be mentioned. (i) the corresponding isosbestic points in the amide I' band at 1667 $cm^{-1}$ and in the amide II' at 1435 $cm^{-1}$, and (ii) the response of a distinct tyrosin population to T-ME.

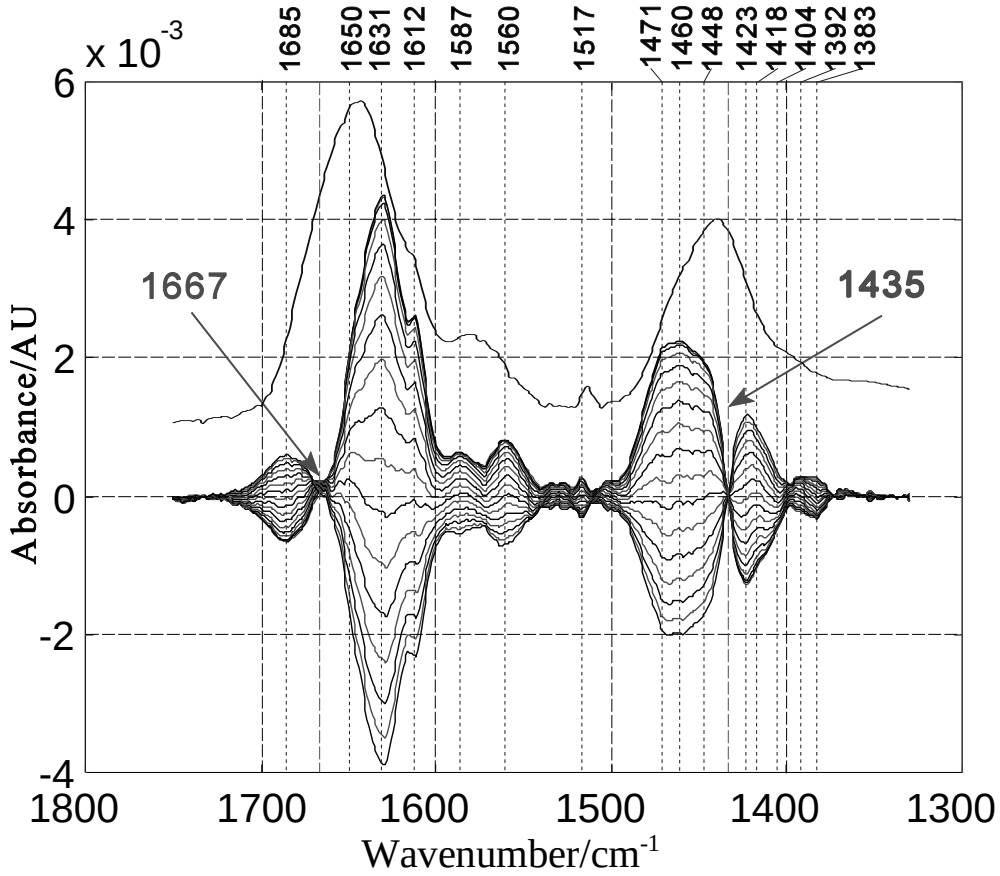


**FIGURE 12.** Stationary (upper trace) and phase resolved (9°) FTIR ATR modulation spectra of temperature modulated excitation of RNase A dissolved in $D_2O$ buffer, pD 7. Mean temperature $\overline{T}$=64°C, modulation amplitude $\Delta T/2$=5°C. Note tyrosin response T-ME is selective, because the responding population absorbs at 2-3 $cm^{-1}$ higher than the supperposition of all tyrosins of RNase. Secondary structural conversion results in isosbestic points in the amide I' and amide II' regions.

In the modulation spectrum, the tyrosin band appears at 1517 $cm^{-1}$, whereas in the stationary spectrum the corresponding band is found to be considerably broader with the peak maximum shifted to lower wavenumbers.

As in the case of PLL the shapes of modulation spectra alter with PSD phase setting $\phi_{PSD}$, indicating that some phase resolution is achieved. The effect, however is less distinct than with PLL. Most probably higher modulation frequencies are required in order to get larger differences in the phase angles $\phi_i$ of different conformational

populations. T-ME-experiments at higher frequencies are in progress.

## ACKNOWLEDGEMENTS

Grant No. 6106 by the Jubiläumsfonds of the Oesterreichische Nationalbank is kindly acknowledged. It enabled scholarships for G.R. and M.S. We thank the University of Vienna for a preceding research scholarship for G.R. International contacts in the framework of the presented projects were facilitated by the EC research project grant No. BIO4-CT96-0022, and support by the Oesterreichischer Aussendienst (ÖAD). Both grants are kindly acknowledged. U.P.F. thanks gratefully to Prof. R. Hütter, former Vice President for research of the Swiss Federal Institute of Technology (ETH) Zurich, for enabling performance of a substantial part of the presented experimental work at the Technopark ETH. The authors are indebted to J. Gast, Dr. A. Simon, Dr. J. Gronholz from Bruker Analytische Messtechnik, Karlsruhe, Germany, and to Dr. W. Tschopp, Dr. A. Marcuzzi and D. Stierli from Spectrospin AG, Fällanden, Switzerland, for technical support. Supply of Creatine kinase by Prof. Th. Wallimann, O. Stachowiak, and U. Schlattner, Institute for Cellular Biology, ETH Zurich, and supply of Alcaline Phosphatase by Prof. B. Roux and Ms. M. Angrand, Laboratoire de Physico Chimie Biologique, University Claude Bernard, Lyon I, Lyon, France, is gratefully acknowledged.

## REFERENCES

1. Tamm, L.K., and McConnell, H.M., *Biophys. J.* **47,** 105-113 (1985).
2. Brian, A., and McConnell, H.M.,*Proceedings of the National Academy of Sciences USA* **81,** 6159-6163 (1984).
3. Fringeli, U. P. in Schlunegger, U.P. (Ed.), *Biologically Active Molecules*; Springer: Berlin, **1989**; pp. 241-252.
4. Fringeli, U. P., in Mirabella, F. M. (Ed.), *Internal Reflection Spectroscopy, Theory and Applications*, Marcel Dekker **1992,** Chpt. 10, 255-324.
5. Kalb, E., Frey, S., and Tamm, L., *Biochim. Biophys, Acta* **1103,** 307-316 (1992).
6. Wenzl, P., Fringeli, M., Goette, J. and Fringeli, U. P., *Langmuir* **10,** 4253-4264 (1994).
7. Schöpflin, M., Perlia, X., and Fringeli, U. P., *J. Am. Chem. Soc.* **109,** 2375-2380 (1987).
8. Jeannette, ATR-IR-spektroskopische Untersuchungen der Lokalanästhetika-Modellmembran-Interaktion und dampfdruckosmometrische Bestimmung der Assoziation von Lokalanästhetika in wässriger Lösung, Zürich: PhD Thesis Nr. 9721, Swiss Federal Institute of Technology (ETH),1992.
9. Goette, J., Fahr, A., and Fringeli, U. P., *Langmuir*, in preparation.
10. Fringeli, U. P., Apell, H.-J., Fringeli, M., and Läuger, P., *Biochim. Biophys. Acta* **984,** 301-312 (1989).
11. Frey, S., and Tamm, *L. K., Biophys. J.* **60,** 922-930 (1991).
12. Fringeli, U. P., and Fringeli, M., *Proc. Natl. Acad. Sci. USA* **76,** 3852-3856 (1979).
13. Stephens, S.M., and Dluhy, *R., Thin Solid Films* **284-285,** 381.-386 (1996).
14. Fritz-Wolf, K., Schnyder, Th., Wallimann, Th., and Kapsch, W., *Nature* **381,** 341-345 (1996).
15. Stachowiak, O., Dolder, M., and Wallimann, Th., *Biochemistry*, **35,** 15522-15528 (1996).
16. Siam, M., Reiter, G., Schwarzott, M., Baurecht, D., and Fringeli, U. P., *"Interaction of two different types of membrane proteins with model membranes investigated with FTIR-ATR spectroscopy"*, presented at the 11th International Conference on Fourier Transform Spectroscopy (ICOFTS-11), Athens, Georgia, U.S.A., August 10-15, 1997. See publication in this book.
17. Siam, M., Stachowiak, O., Schlattner, U., Wallimann, Th., and Fringeli, U. P., in preparation.
18. Reiter, G., Angrand, M., Roux, B., and Fringeli, U. P., in preparation.
19. Fringeli, U. P., *Simultaneous phase-sensitive digital detection process for time-resolved, quasi-simultaneously captured data arrays of a periodically stimulated system*, PCT international patent application, WO97/08598, 1997.
20. Müller, M., Buchet, R., and Fringeli, U. P., *J. Phys. Chem.* **100,** 10810-18825 (1996).
21. Reinstädler, D., Fabian,H., Backmann, J., and Naumann D., *Biochemistry* **35,** 15822-15830 (1996).
22. Born, M., and Wolf, E., *Principles of Optics*, Oxford: Pergamon Press, 1983, 6th ed. Ch. 1, pp. 47-51.
23. Harrick, N. J., *Internal Reflection Spectroscopy*, New York: Interscience Publisher, 1967.
24. Fringeli, U. P., *Chimia* **46,** 200-214 (1992).
25. Ritchie, J. M.,and Green, N. M., *Local Anesthetics*, in: Gilman, A. G., Goodman, L. S., and Gilman, A., Eds., *The Pharmacological Basis of Therapeutics*, New York: Macmillan Publishing, 1990, 7th Ed.
26. Seelig, A., Allegrini, P. R., and Seelig, J., *Biochim. Biophys. Acta* **939,** 267-276 (1988).
27. Del Zoppo, M., and Zerbi, G., *Polymer*, **33,** 4667-4672 (1992).
28. Mantsch, H. H., and McElhaney, R. N., *Chem. Phys. Lipids* **57,** 213-226 (1991).
29. Fringeli, U. P., and Günthard, Hs. H., *Biochim. Biophys. Acta* **450**, 101-106 (1976).
30. Fringeli, U. P., and Günthard, Hs. H. "Infrared Membrane Spectroscopy", in: "Membrane Spectroscopy", E.Grell ed.,Springer 1981, pp. 270-332.
31. Fringeli, U. P., and Hofer, P., *Neurochemistry International* **2,** 185-192 (1980).
32. Roberts, *Thin Isolating Films on Semi-Conductors*, Springer Heidelberg, 1981.
33. Fringeli, U. P., Schadt, M., Rihak, P., and Günthard, Hs. H., *Z.Naturforsch.* **31a,** 1098-1107 (1976).
34. Baurecht, D, Neuhäusser, W., and Fringeli, U. P., presented at the 11th International Conference on Fourier Transform Spectroscopy (ICOFTS-11), Athens, Georgia, U.S.A., August 10-15, 1997. See publication in this book.
35. Forster, M., Loth, K., Andrist, M., Fringeli, U.P., and Günthard, Hs.H., *Chemical Physics* **17,** 59-85 (1976).
36. RNase A project: Collaboration with Dieter Naumann and Diane Reinstädler, Robert Koch Institute, Berlin, Germany.